Geophys. J. Int. (2005) **160,** 127–143 doi: 10.1111/j.1365-246X.2005.02354.x

Shear velocity structure in the Aegean area obtained by inversion of Rayleigh waves

E. E. Karagianni,[1] C. B. Papazachos,[1] D. G. Panagiotopoulos,[1] P. Suhadolc,[2] A. Vuan[3] and G. F. Panza[2,4]

[1] *Geophysical Laboratory, Aristotle University of Thessaloniki,* PO Box 352-1, GR 54006, *Greece. E-mail: karagian@lemnos.geo.auth.gr*
[2] *Department of Earth Sciences, University of Trieste, Italy*
[3] *Centro Ricerche Sismologiche, Intituto Nazionale di Oceanografia e di Geofisica Sperimentale, Trieste, Italy*
[4] *The Abdus Salam International Centre for Theoretical Physics, SAND Group, Trieste, Italy*

Accepted 2004 April 15. Received 2004 April 15; in original form 2003 January 21

SUMMARY

The purpose of this work is to derive a 3-D tomographic image of the shear wave velocity structure of the crust—uppermost mantle in the Aegean area using the group velocities of Rayleigh wave fundamental mode. The database consists of 185 regional earthquakes recorded at broad-band stations that were installed for a period of 6 month in the Aegean area within the framework of a large-scale experiment. In a previous work (Karagianni *et al.* 2002), an averaged group velocity has been determined using the method of frequency time analysis (FTAN) for each epicentre–station ray path and the data were used in order to determine the local group velocities for different periods over the area covered by the seismic ray paths. Taking into account additional resolution results obtained for the local group velocities, a grid of 0.5° was adopted for the Aegean area and a local dispersion curve was defined for each gridpoint. More than 80 local dispersion curves were finally inverted using a non-linear inversion approach, deriving the corresponding 1-D shear velocity models. The interpolation of these models resulted in a 3-D *S*-wave tomographic image of the crust and uppermost mantle in the broader Aegean area. As expected, as a result of the complex tectonic setting of the Aegean area, strong lateral variations of the *S*-wave velocities of the crust and uppermost mantle of the studied area are found. In the southern Aegean sea, as well as in a large part of the central Aegean sea a thin crust of approximately 20–22 km is observed, whereas the remaining Aegean sea area exhibits a crustal thickness less than 28–30 km. On the contrary, a crustal thickness of 40–46 km is observed in western Greece along the Hellenides mountain range, whereas in the eastern continental Greece the crust has a typical thickness of approximately 30–34 km.

For shallow depths (<10 km) low *S*-wave velocities are observed under the sedimentary basins of the north Aegean sea, the Gulf of Thermaikos (Axios basin) and western Greece. At depths ranging from 10 to 20 km, low *S*-wave velocities are mainly found in western Greece under Peloponnesus as well as in Rhodes. This low-velocity zone seems to extend along the Hellenic arc and can be correlated to the Hellenides mountain range and the Alpine orogenesis, in agreement with previous *P*-wave tomographic results. In the southern Aegean sea very low *S*-wave velocities (3.6–4.0 km s^{-1}) are observed at depths of approximately 30–40 km just below the Moho discontinuity, while in the rest of the inner Aegean sea and continental Greece the uppermost mantle is characterized by velocities around 4.3–4.4 km s^{-1}. This low-velocity zone in the southern Aegean sea can be associated with the high temperatures and the presence of significant percentage partial melt in the mantle wedge of the southern Aegean subduction zone, in agreement with previous studies.

Key words: Aegean area, group velocity, Hedgehog inversion, Moho, Rayleigh waves, shear wave velocity structure.

1 INTRODUCTION

The Aegean region is an area of complex tectonics that lies at the convergence zone of the Eurasian and African lithospheric plates. The Eastern Mediterranean Plate is subducting under the Aegean, which has been recognized to form a separate Aegean microplate moving at an average velocity of $\sim$ 35–40 mm yr^{-1} towards the southwest with respect to Eurasia (McKenzie 1972; Jackson 1994; Papazachos *et al.* 1998; Papazachos 1999). McClusky *et al.* (2000) using geodetic measurements found that the southwestern Aegean–Peloponnesus moves towards the S–SW relative to Eurasia, at 30 $\pm$ 2 mm yr^{-1} in a coherent fashion, with low internal deformation (<2 mm yr^{-1}). The subduction that takes place in the eastern Mediterranean results in the formation of a well-defined Benioff zone (Papazachos & Comninakis 1969; Caputo *et al.* 1970; McKenzie 1970; Papazachos & Comninakis 1971; McKenzie 1978; Le Pichon & Angelier 1979). Moreover, it is the main reason behind the high tectonic activity in this area, with volcanic activity (e.g. Georgalas 1962), magnetic anomalies and positive isostatic anomalies (e.g. Fleischer 1964; Vogt & Higgs 1969; Makris 1976), high heat flow (e.g. Fytikas *et al.* 1985) and high attenuation of seismic energy (e.g. Papazachos & Comninakis 1971; Hashida *et al.* 1988). Fig. 1 shows the main topographic features of tectonic origin and stress field characteristics in the study area (modified from Papazachos & Papazachou 1997). The main zone of compression with thrust faults, which are observed along the Hellenic arc and along the western coast of northern Greece and Albania, is associated with the subduction of the eastern Mediterranean beneath the Aegean and the continental–continental type collision between the Adriatic (Apulia) microplate and the western Greek–Albanian coasts (Anderson & Jackson 1987). A dextral strike-slip zone (North Anatolia Fault – NAF) is found in the North Anatolia—North Aegean trough (McKenzie 1970, 1972; Taymaz *et al.* 1991), which seems to be continued to the Kefallonia area (Scordilis *et al.* 1985). The largest part of the backarc Aegean area is dominated by normal faults with an E–W trend, suggesting an N–S extension. Finally, a narrow zone of E–W extension lies between the thrust faults of the outer Hellenic arc and the N–S extension field in the backarc area, as has been identified using fault plane solutions (e.g. Papazachos *et al.* 1984; Kiratzi *et al.* 1987; Papazachos *et al.* 1998), as well as by recent GPS measurements (McClusky *et al.* 2000). The volcanic arc, which is one of the characteristic features of the subduction, is parallel to the external sedimentary arc at a mean distance of 120 km (Papazachos & Comninakis 1971). The distribution of the

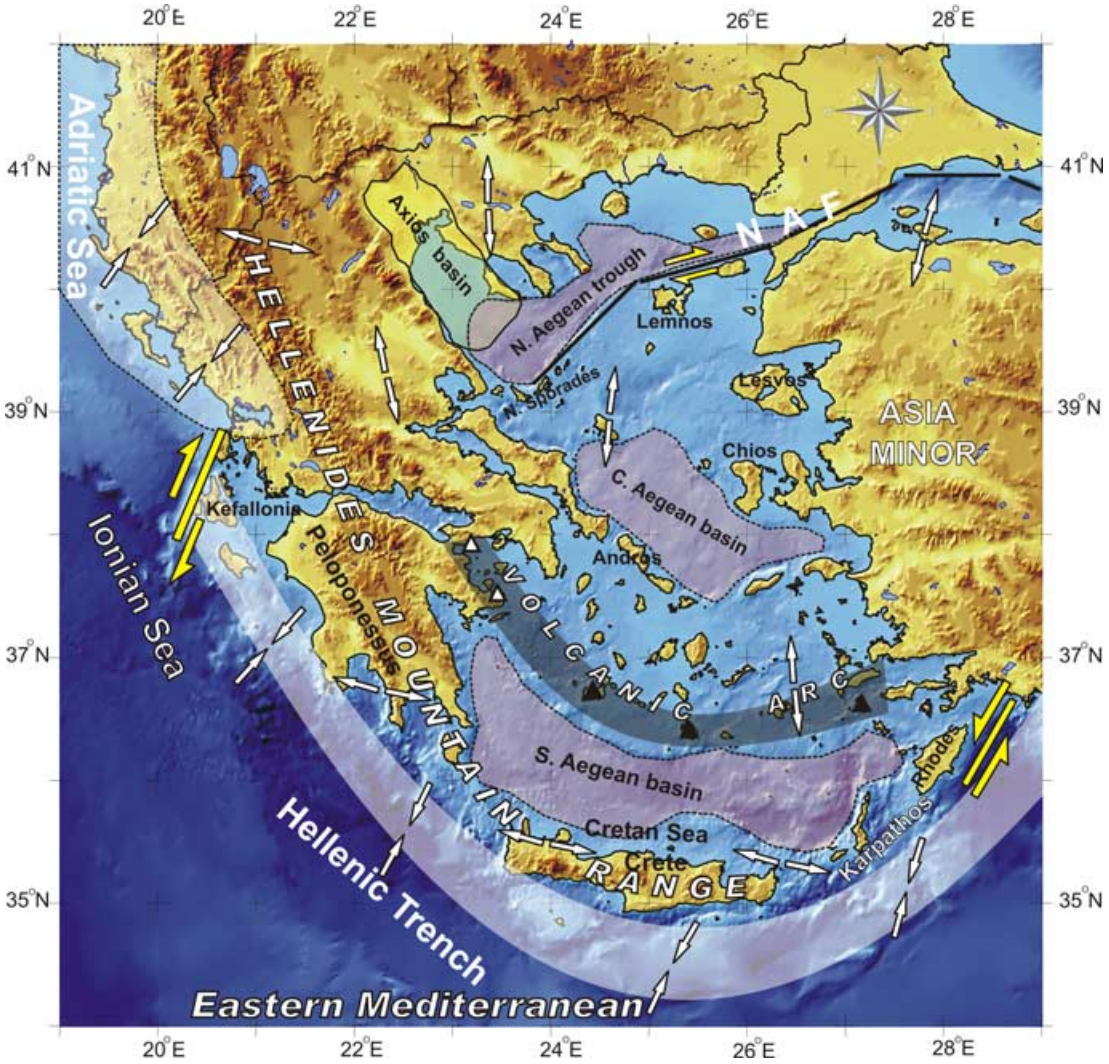

Figure 1. Main features of tectonic origin in the broader Aegean region (modified from Papazachos & Papazachou 1997).

volcanism in the Aegean area is strongly correlated with the intermediate depth seismicity at this area. The tectonic processes that occur in the subducting slab in the Aegean area control both the distribution of the volcanism and the melt generation in the mantle. This suggests that melt generation is concentrated in zones above those parts of the slab that are heavily deformed and where pore fluids from dehydration reactions are focused to be released into the mantle wedge via hydraulic fraction. It is inferred that fluids from dehydration reactions within the slab are channelled towards the slab–wedge interface by faults in the slab segment boundaries. Subsequently, focused slab fluids are released into hotter regions of the mantle wedge via hydraulic fracturing. The result is an increased melt generation in those parts of the mantle wedge that overlie the fracture zones and the location of the recent volcanic activity in the south Aegean (e.g. Zelimer 1998; Papazachos *et al.* 2004).
In Fig. 1, the main sedimentary basins, such as the basin of Axios with a maximum thickness of sediments of approximately 10 km (Roussos 1994) and the North Aegean trough with a sedimentary thickness of approximately 6 km (Kiriakidis 1988), are also shown. In the same figure, the main characteristics of the Hellenic arc, such as the volcanic arc, the sedimentary arc (Hellenides mountain range), the Southern Aegean basin and the Hellenic trench, are also shown.

The velocity structure of the crust and upper mantle in this area has been extensively studied and most such studies are mainly based on the propagation of *P* waves. Traveltimes of body waves generated by either earthquakes (Panagiotopoulos 1984; Panagiotopoulos & Papazachos 1985; Plomerova *et al.* 1989) or by explosions (Makris 1973, 1978; Delibasis *et al.* 1988; Voulgaris 1991; Bohnhoff *et al.* 2001) have been used for the study of the velocity structure under the Aegean area. Moreover, an overall description of the 3-D lithosphere and upper-mantle *P*-wave structure is given by various tomographic studies (e.g. Spakman 1986; Christodoulou & Hatzfeld 1988; Spakman *et al.* 1988; Drakatos 1989; Drakatos *et al.* 1989; Ligdas *et al.* 1990; Drakatos & Drakopoulos 1991; Ligdas & Main 1991; Ligdas & Lees 1993; Spakman *et al.* 1993; Papazachos *et al.* 1995; Tiberi *et al.* 2000). Recently, Papazachos & Nolet (1997) used traveltime data from local earthquakes in Greece and surrounding areas and presented detailed results for the 3-D *P* and *S* velocity structure of the Aegean lithosphere. Gok *et al.* (2000) provided an attenuation study of regional shear wave (Sn and Lg) in the northern Aegean and Greek mainland area and showed that an inefficient Sn propagation along the volcanic arc as a result of the low upper-mantle velocities is observed in this area. Hatzfeld *et al.* (2001) studied the shear wave anisotropy in the upper mantle beneath the Aegean area and found that the seismic anisotropy is not restricted to the North Anatolian fault but is distributed over a region several hundreds kilometres away. According to their results, little anisotropy is observed along the Hellenic arc and in continental Greece, whereas significant anisotropy is observed in the north Aegean sea.

The published results on the lithospheric structure based on measurements of the dispersion of surface waves are more limited. The early works of Papazachos *et al.* (1967) and Papazachos (1969) used group and phase velocities of Love and Rayleigh waves and studied the structure of the southeastern and eastern Mediterranean region, respectively. Payo (1967, 1969) studied the structure of the Mediterranean sea region using dispersion measurements of surface waves and identified a significant difference in the crust between eastern and western Mediterranean area, while Calcagnile & Panza (1980) and Calcagnile *et al.* (1982) focused on the regional study of the lithosphere–asthenosphere structure in the Mediterranean region. More recently, Kalogeras (1993) and Kalogeras & Burton (1996) used group velocity measurements of Rayleigh waves and studied the shear wave velocity structure down to 60–70 km along some seismic ray paths in the broader Aegean area. Marquering & Snieder (1996) used a waveform inversion method, where the synthetic seismograms are calculated taking surface wave coupling and studied the *S*-wave velocity structure beneath Europe, western Asia and NE Atlantic up to a depth of 670 km. They showed that in Central Europe, where the ray density is highest, small-scale structures are recovered, such as the presence of high velocities associated with the Hellenic subduction zone. Moreover, Yanovskaya *et al.* (1998) studied the shear wave velocity structure under the Black sea and surrounding regions using surface wave group velocities. Martinez *et al.* (2000) studied the shear velocity structure of the lithosphere–asthenosphere system under the broader Mediterranean area using group velocities derived from the Rayleigh wave fundamental mode, while Pasyanos *et al.* (2001) investigated the broader southern Eurasia and the Mediterranean sea region using group velocities of both Rayleigh and Love waves.

In general, previous studies in the broader Aegean area show the existence of strong variations in the crustal structure that characterize this region but are usually of limited spatial resolution. A thin crust approximately 20–30 km thick has been proposed for the backarc area, whereas a significant crustal thickness (40–47 km) has been identified along the Hellenides mountain range. The crust has a normal thickness (28–37 km) in the eastern part of the Greek mainland, in the northern and central Aegean, in western Turkey and in Crete.

The 3-D *S*-wave velocity structure is not well-known for the Aegean as a result of the very limited number of tomographic studies that employ *S* arrivals. The main purpose of this paper is to obtain a detailed 3-D tomographic image of *S*-wave velocity for the uppermost $\sim$ 50 km in the Aegean area. For this purpose, Rayleigh wave group velocities along different ray paths have been estimated, using the vertical components of the waveforms from which a data set of approximately 800 dispersion curves covering the studied area has been extracted (Karagianni *et al.* 2002). Using these data, group velocity tomographic maps for different periods, ranging from 5 to 30 s have been constructed and inverted in order to determine the 3-D *S*-wave velocity structure of the examined area.

2 ANALYSIS OF SURFACE WAVE DATA

2.1 Tomographic method

For each epicentre–station seismic ray path, an averaged group velocity curve of the fundamental mode of Rayleigh wave is estimated for the period range from 5 to 30 s, using the method of frequency time analysis (FTAN) developed by Levshin *et al.* (1972, 1989, 1992). The group velocities along different ray paths have been used to construct the group velocity tomographic maps at different periods.

To construct the group velocity tomographic maps, a generalized 2-D linear inversion program developed by Ditmar & Yanovskaya (1987) and Yanovskaya & Ditmar (1990) has been applied. The method of Yanovskaya and Ditmar is a generalization to two dimensions of the classical 1-D method of Backus & Gilbert (1968). The result of surface wave tomography is the estimation of local values of group velocity at different gridpoints over the studied area, which can be used to obtain group velocity maps for different periods.

In tomography, the knowledge of the resolution is important in order to estimate the minimum resolvable feature for a given sample

and to determine those features that may be a numerical artefact. Yanovskaya (1997) and Yanovskaya *et al.* (1998) proposed the use of two parameters as resolution measures. The first resolution parameter is the mean size of the averaging area, L, given by

$$L = [s_{\min}(x, y) + s_{\max}(x, y)]/2, \quad (1)$$

where $s_{\min}(x, y)$ and $s_{\max}(x, y)$ are the smallest and the largest axes of an ellipse that the averaging area can be approximated to, centred at each examined point (x, y). As the resolution is closely correlated to the density of the crossing ray paths in each cell, it is clear that small values of the mean size of the averaging area (corresponding to high resolution) should appear in the areas that are crossed by a large number of ray paths and vice versa.

The second parameter is the stretching of the averaging area, which provides information on the azimuthal distribution of the ray paths and is given by the ratio

$$2[s_{\max}(x, y) - s_{\min}(x, y)]/[s_{\max}(x, y) + s_{\min}(x, y)]. \quad (2)$$

Small values of the stretching parameter imply that the paths are more or less, uniformly distributed along all directions, hence the resolution at each point can be represented by the mean size of the averaging area. On the contrary, large values of this parameter (usually >1) mean that the paths have a preferred orientation and that the resolution along this direction is likely to be quite small (Yanovskaya 1997).

2.2 Inversion method

The non-linear inversion method applied for the determination of the velocity structure using the dispersion curve is known as the Hedgehog method (Keilis-Borok & Yanovskaya 1967; Valyus 1968; Knopoff 1972; Biswas & Knopoff 1974; Calcagnile & Panza 1980; Panza 1981). The Earth model is parametrized by the density and the *P*- and *S*-wave velocities as a discrete function of depth. The parameters may be varied or held fixed in the inversion and can be either independent or dependent, on the basis of *a priori* knowledge. For the independent parameters acceptable models are sought, whereas the dependent parameters maintain a fixed relationship with the independent ones. Because the partial derivatives of phase and group velocity with respect to the shear wave velocity are much larger than those with respect to the compressional wave velocity and density (e.g. Urban *et al.* 1993), only the *S*-wave velocity and the layer thicknesses were chosen as independent parameters. Each parameter to be inverted is specified to vary within a particular range, with upper and lower bounds. For a given model, a set of theoretical values (group velocities in the present study) are computed with the Knopoff method (Knopoff 1964; Schwab & Knopoff 1972; Schwab *et al.* 1984). Starting from the largest period, the theoretical group velocity is computed and compared with the observed value. If the difference lies within the observational errors (single point error) the inversion proceeds to test the next shorter period and so on. If this test fails at any individual period, the model is rejected and a new model in the neighbourhood of the previous one is tested. If the test is successful at all individual periods of the dispersion curve, the rms difference (root-mean-square deviation) between theoretical and observed values of group velocity is computed and compared with a preset value (usually less than 0.06 km s^{-1}). After tests, the preset value was set at 60 per cent of the experimental error of the group velocity values and was used in order to avoid the large jumps of the theoretical dispersion curves or avoid solutions with a systematic bias with respect to the experimental curve. Models that pass both criteria are acceptable and the same process is repeated until the neighbourhood around each satisfactory combination of the search parameters is explored.

3 DATA SELECTION AND PROCESSING

In the present study, group velocities of the fundamental mode of Rayleigh waves that travelled across the Aegean area have been used as initial data. We have considered regional earthquakes within the area defined by 34° –42° N and 19° –31° E, which were recorded by the broad-band stations of a temporary network that has been installed in the Aegean area for a period of 6 month. The locations of the events, as well as of the portable stations are shown in Fig. 2(a), while a detailed description of these data is given in a previous paper (Karagianni *et al.* 2002).

Around 800 observed Rayleigh wave group velocities have been finally determined along different ray paths covering the region under study. The frequency bandwidth of each measurement depends on the ability of the analyst to identify the direct fundamental mode arrival and to distinguish it from higher modes, other reflections or coda waves. As the mean path length is of the order of 400 km, the Rayleigh waves have been well recorded in the period range from 5 to 30 s. The coverage of the study area for the period of 10 s is shown in Fig. 2(b). The azimuthal distribution of the paths is quite uniform and the coverage is satisfactory, especially in the central Aegean area where a large number of portable stations were located. Poorer density of seismic ray paths is observed in western Greece, NNE Greece and SW Crete as a result of the lack of earthquakes and recording stations.

3.1 Lateral variations of Rayleigh wave group velocities

The group velocity maps over the Aegean area for the periods ranging from 5 to 30 s are presented in detail in Karagianni *et al.* (2002) and will be only briefly discussed here. In Fig. 3, the group velocity variation for two selected periods (10 and 24 s) is presented. In general, the group velocity maps show significant lateral velocity heterogeneity with variations up to 30 per cent in the study area.

For shorter periods (6–14 s) the observed velocity anomalies mostly correlate with shallow geological features (Fig. 1). In particular, the most important features identified in the group velocity maps as significant low-velocity anomalies correlate well with a number of known structural features. Examples include the big thickness of sediments under the Hellenides mountain range in western Greece, the sedimentary basin of Axios in northern Greece continuing to the North Aegean trough and the Southern Aegean basin with its high observed heat flow (Fig. 3a). At the largest periods (19–28 s) an increase in group velocity values is observed. For the period of 24 s, the large lateral differences in group velocity values suggest a significant difference in the crustal thickness between western Greece and the inner Aegean sea (Fig. 3b).

The standard errors associated with the local group velocities range from 0.04 to 0.09 km s^{-1} for all the examined periods (Karagianni *et al.* 2002). Furthermore, the mean size of the averaging area (quantifying the resolution of the local group velocity distribution) is of the order of 50–100 km in the central part of the Aegean and becomes poorer (∼200 km) only at the borders of the maps, where the path coverage is limited. The values of the stretching parameter of the averaging area generally indicate that the azimuthal distribution of the paths is quite uniform. In Fig. 3, the results are presented

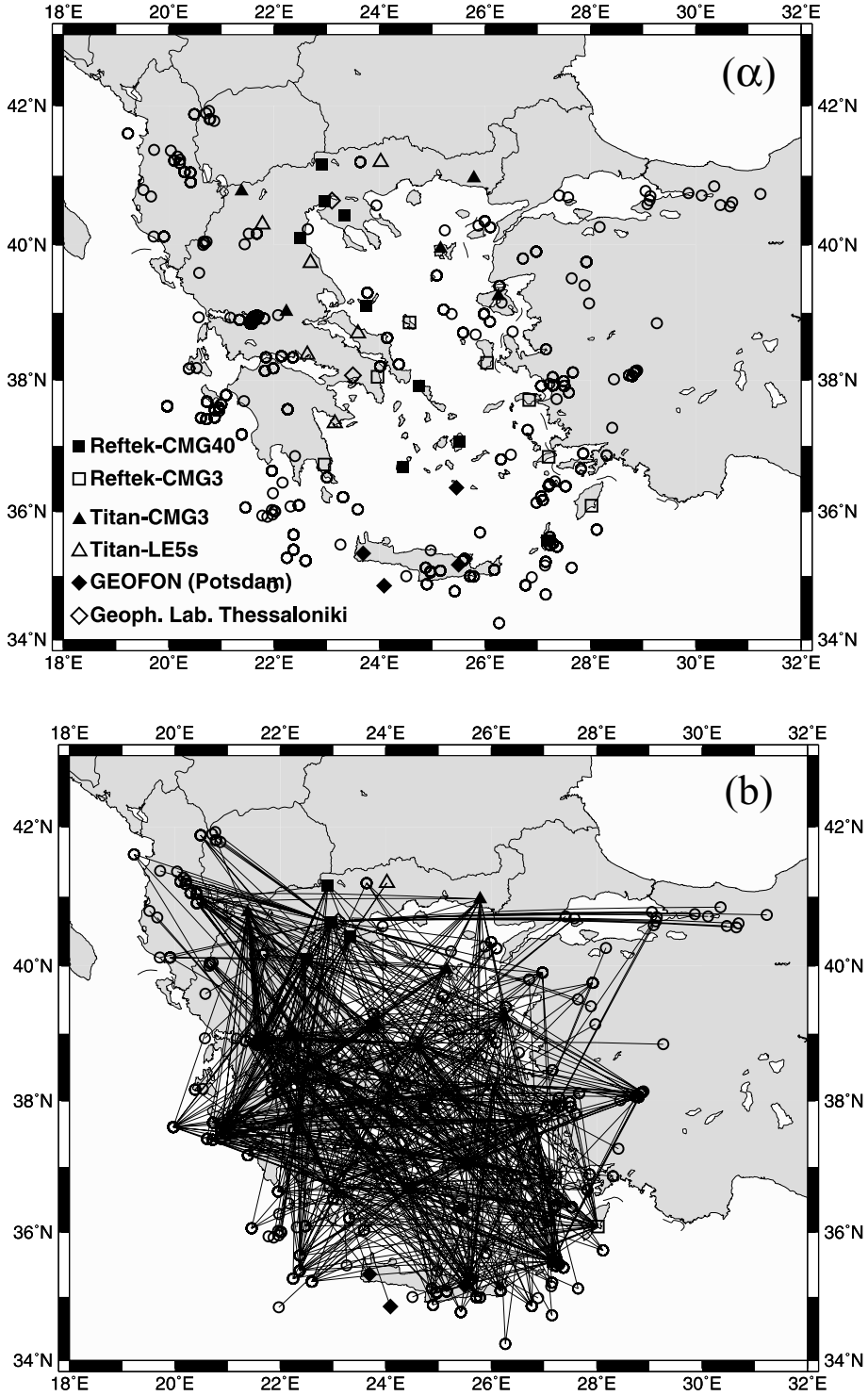

Figure 2. (a) Map of the epicentres (open circles) of the events used in this study and the locations of the portable stations. (b) Path coverage of the ray paths used in this study for the period of 10 s.

only for areas where the mean size of the averaging area is less than 200 km.

In order to further validate the results obtained by Karagianni *et al.* (2002), we have performed additional checkerboard tests. For this reason, the study area was divided into cells and a velocity perturbation of ± 20 per cent with respect to the average group velocity for each examined period was assumed for the cells. Using this model, traveltimes along paths linking source and recording stations were calculated, adopting the same ray coverage configuration as in Fig. 2. A solution for these velocity perturbations was obtained using the same regularization parameter, a, as for the real data in the tomographic inversion. The checkerboard test was performed for different cell sizes, as well as for different values of velocity perturbation. The results show that tectonic features with sizes ∼100 km or less in the studied area can be well resolved by the real data for the largest part of the study area. In Fig. 4(a), we show the re-

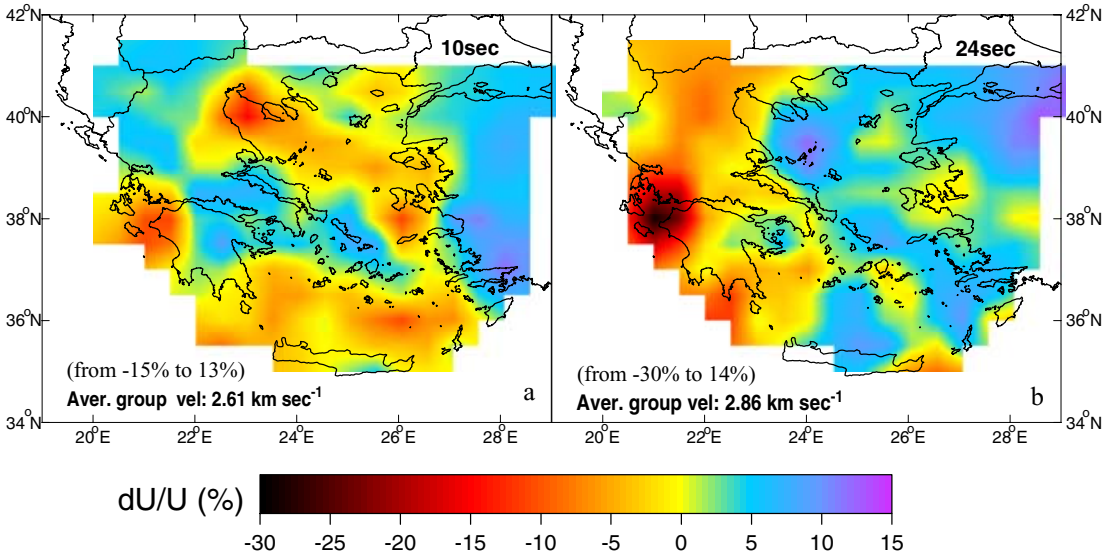

Figure 3. Estimated Rayleigh wave group velocity maps at two selected periods. Maps depict lateral variations (in per cent) of group velocity, relative to the average group velocity for each plot.

sults of the checkerboard test for the period of 10 s. Moreover, in Fig. 4(b) we present the contour lines of 100 and 150 km for the mean size of the averaging area of the real data (eq. 1), which define the region of the acceptable resolution. In the same figure, we have added for comparison the well-resolved model area, as defined from the checkerboard tests for two different cell dimensions (1° × 1°/∼100 × 100 km, 1.5° × 1.5°/∼150 × 150 km) and two periods (10 and 24 s). It is clear that the well-resolved area according to the checkerboard tests is in very good agreement with the values of the mean size of the averaging area that have been presented in the previous work of Karagianni *et al.* (2002). Furthermore, Fig. 4(b) shows that resolution is similar for both high (10 s) and low (24 s) frequencies, hence local group velocity curves can be reliably constructed and inverted for each cell.

From the group velocity maps a grid of 0.5° × 0.5° has been defined over the Aegean area and a local group velocity has been estimated for every gridpoint. Using the local group velocities for different periods between 5 and 30 s as derived from the tomographic maps calculated in the previous work of Karagianni *et al.* (2002), a local dispersion curve has been constructed for each gridpoint. Finally, a mean local dispersion curve was assigned to each cell defined by the grid, using the dispersion curves that corresponded to the four corners of each cell.

3.2 Inversion results

In the present work, the inversion scheme has been applied to 80 mean local dispersion curves over the Aegean area, producing vertical 1-D shear wave velocity models for each examined gridpoint. After the inversion, a simple linear interpolation scheme between the centres of the cells was adopted and a 3-D image of the *S*-wave structure of the Aegean area was derived for depths ranging from 5 to 45 km.

Even if with the adopted non-linear inversion scheme, the starting model does not significantly affect the final results, the starting model of *S*-wave velocities for the inversion have been taken from the work of Papazachos & Nolet (1997). This and the work of Martinez *et al.* (2000) are the only tomographic works that give detailed information on the 3-D *S*-wave velocity structure of the Aegean lithosphere. For the cases where the inversion was performed at gridpoints in the sea, the starting 1-D model was overlain by a water layer of variable thickness (0.2–2.5 km), according to the bathymetric map for the broader Aegean area.

Because group velocity data were available only for the range 5–30 s, it is not possible to resolve the parameters of the very shallow layers, as well as those of the deep mantle. For this reason the elastic properties for the upper 3–5 km have been fixed on the basis of information coming mainly from seismic soundings performed by the Greek Public Petroleum Company (Roussos, personal communication, 2000) and from other existing geophysical investigations (e.g. Roussos 1994; Makris 1976, 1977; Martin 1987). The *P*-wave velocities have been defined on the basis of *S*-wave velocity values, using the V_p/V_s ratio values given by Papazachos & Nolet (1997). The density values that were used in the present study have been calculated from the values of *P*-wave velocities using the relationship of Barton (1986) for the crustal and the upper-mantle material. We have verified that small modifications in the upper 3–4 km do not have a critical influence on the results of our inversion, because we limited the shorter period of our group velocity data at 6 s. We have performed several tests where the *S*-wave velocities of the shallow layers (usually sedimentary) have been modified up to 0.5 km s^{-1} and the corresponding thicknesses up to 0.5–1 km. All the tests showed that in the inversion results the imposed modifications resulted in variations of the *S*-wave velocities of the order of 0.02–0.09 km s^{-1} for the depths ranging from 5 to 45 km, whereas the Moho depth varied by 1 km at most.

Finally, for each examined geographical point, 8 to 10 parameters have been allowed to vary in the inversion scheme, namely the *S*-wave velocities in 4–5 layers reaching a depth of approximately 40–45 km and the related thicknesses. The steps for the variation of the velocity parameters during the inversion process have been estimated according to the resolving power of the information contained in the available data (Panza 1981).

In Table 1, we show the parametrization that was used in the inversion scheme for a typical gridpoint (E in Fig. 13). The inversions results for this point are shown in Fig. 5, where thick lines present the accepted models that satisfy the criteria of inversion (single point error ∼ 0.07 km s^{-1}, rms deviation ∼ 0.05 km s^{-1}) and thin lines

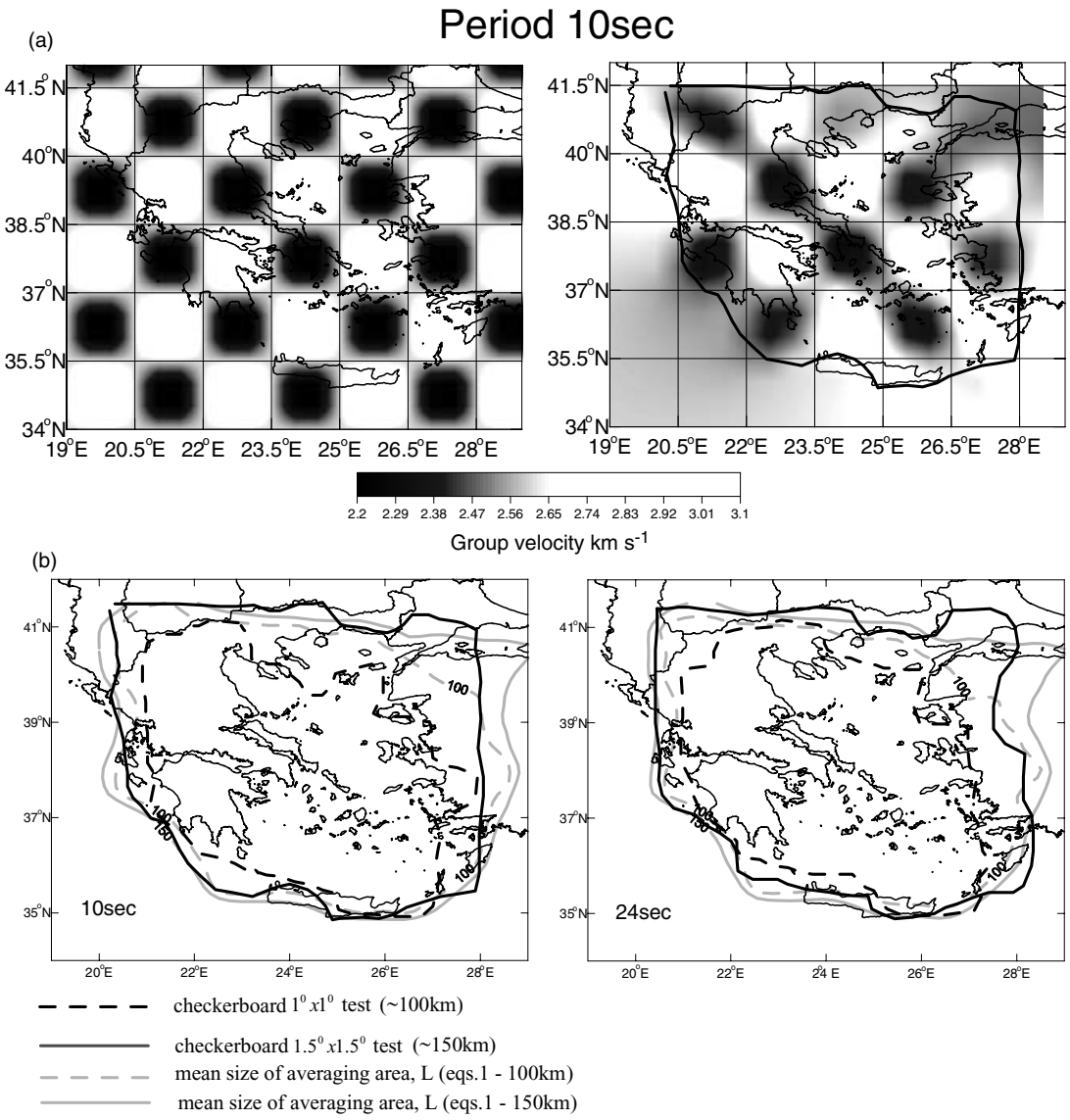

Figure 4. (a) Checkerboard test for 10 s Rayleigh wave with cell 1.5° × 1.5° where the velocity perturbation in the cells is ± 20 per cent. (b) Comparison of resolution lengths obtained from checkerboard tests (black lines) and averaging area (eq. 1) calculations (grey lines) for the periods of 10 and 20 s.

show all the rejected models that were tested in the inversion scheme. The inversion process tested 7314 models but the accepted solutions were only 16, even though that the initials bounds on each parameter are very broad. It is clear that the step adopted for layer thickness, as well as for the *S*-wave velocity variation, was small enough in order not to limit the number and range of the tested models.

In the inversion process for each examined point, we considered the depth of 45–50 km as a maximum depth at which the independent parameters were allowed to vary. This is based upon the variation of the group velocity sensitivity on the shear wave velocity versus depth (Panza 1981; Urban *et al.* 1993), as was already shown in detail in the previous work of Karagianni *et al.* (2002).

4 *S*-WAVE VELOCITY MODELS AND INTERPRETATION

The local 1-D vertical models of shear wave velocity as derived from the inversion process for each examined geographical point have been used in order to construct a detailed map of the Moho depth discontinuity for the study area. For this purpose, we have assumed that a shear wave velocity of approximately 3.9–4.0 km s^{-1} is a reasonable approximation for the *S*-wave velocity at the bottom of the lower crust. Using all the solutions of the inversion, the average *S*-wave velocity was estimated using a depth interval of 2 km in order to define the average *S* velocity depth profile at each point. At this stage, the depth at which we observe a jump in the *S*-wave velocity (from 3.9 to 4.3 km s^{-1}) was taken as the Moho depth. In some cases no jump could be resolved, but a rather smooth transition in *S*-wave velocity from the lower crust to the upper mantle is noticed, in agreement with previous results by Calcagnile *et al.* (1982).

Significant lateral changes in the crustal thickness can be observed in Fig. 6, as is expected from the tectonic complexity of the Aegean region. A large crustal thickness of approximately 40–45 km is found in western Greece along the Hellenides mountain range, whereas a thin crust of approximately 20–22 km is observed between Crete and the volcanic arc (Cretan sea). The thin crust in the southern Aegean sea is in agreement with the N–S extension

Table 1. Parametrization used in the inversion scheme for the geographical point E (Fig. 12). P1, P2, P3, P4, P5, P6 are the independent parameters that could be varied during the inversion scheme with their range and the step variation (in brackets). (P1 is the thickness of the first layer, P2 is the thickness of the second layer, which in this case is the same for the third layer too, P3–P6 are the *S*-wave velocities at the corresponding layers).

h (km)	β(km s^{-1})
0.2	0.0
1	1.6
1.5	2.27
P1	P3
P2	P4
P2	P5
45-P1-2P2	P6
26	4.51
20	4.43
20	4.42
20	4.49

P1 = 3.0 (2.0) 13.0 km
P2 = 4.0 (2.0) 14.0 km
P3 = 2.49 (0.15) 4.00 km s^{-1}
P4 = 2.59 (0.15) 3.99 km s^{-1}
P5 = 2.69 (0.15) 4.91 km s^{-1}
P6 = 2.99 (0.15) 4.999 km s^{-1}

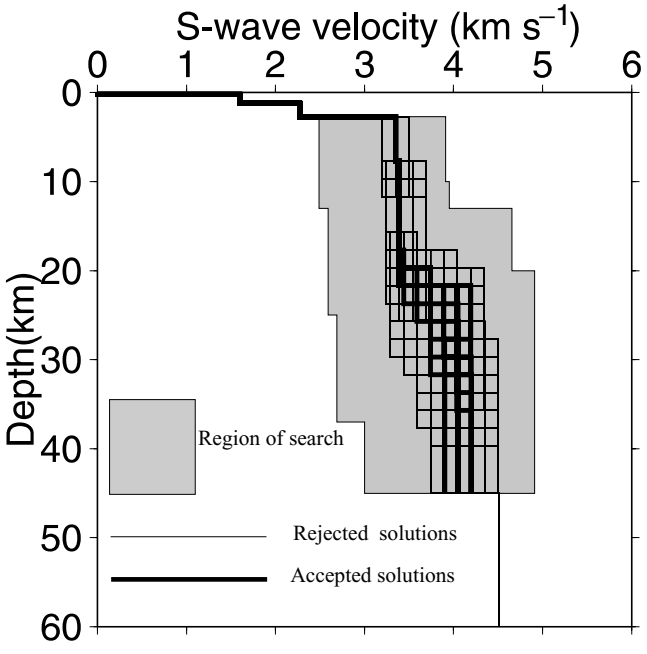

Figure 5. Accepted (thick line) and rejected (thin line) models of *S*-wave velocity obtained from the Hedgehog inversion for a typical gridpoint in north Aegean sea (point E, Fig. 12).

field (Fig. 1), as well as with the rise of the hot mantle material as a result of the subduction of the eastern Mediterranean plate under the Aegean microplate. A thin crust of approximately 20–22 km is also observed in the central Aegean sea between the islands of Andros and Chios. The largest part of the Aegean sea shows a crustal thickness less than 28–30 km, except for the area north of Lemnos island, where a crust with a thickness of approximately 32–34 km is locally observed. The north Aegean sea is characterized by a thin crust and a crustal thickness of approximately 25 km is observed near the North Sporades islands. The aforementioned results are in agreement with previous investigations (e.g. Makris 1976; Brooks & Kiriakidis 1986; Chailas *et al.* 1993; Papazachos 1994, 1998).

In Fig. 7(a), we show the estimated error of the Moho depth discontinuity in kilometres, as this has been constructed by studying the dispersion of Moho depths derived from all the accepted solutions at the gridpoints where the inversion has been performed. It is observed that for the largest part of the studied area the estimated error is less than 4 km, which is acceptable considering the wide range that the Moho depth discontinuity was allowed to vary during the inversion. At the borders of the studied area, the error of our results becomes larger as the data coverage (group velocity along different ray paths) is poor, hence results at the borders may still be questionable. For two randomly selected points where the inversion scheme has been applied (points I and B in Fig. 12), we show the histograms (Fig. 7b) of the values of the computed Moho depth discontinuity, where most of the solutions suggest that the Moho depth is around 35–36 and 21–22 km, respectively.

Significant lateral variations for the shear wave velocities are also detected, as can be seen from the horizontal velocity distributions presented in Fig. 8. For example, in the depth range from 20 to 26 km, *S*-wave velocities of the order of 3.2 km s^{-1} are detected in western Greece, whereas an *S*-wave velocity of approximately 4.2 km s^{-1} is observed in the southern and part of the central Aegean sea.

Most of the shallow depths sections (6–16 km) are dominated (Peloponnesus, north and western Greece, south Aegean sea) by relatively low *S*-wave velocities. These low velocities are in agreement with the results of Kalogeras (1993), who indicated comparable velocities at a depth of approximately 12 km along two paths of SW Peloponnesus—Athens and SW Crete—Athens. The observed velocity zones have the well-known Dinaric trend (NNW–SSE), which is expressed in northwest Greece by the Hellenides mountain range, which changes to east–west in western Turkey and ENE–WSW in the central and southern Aegean sea. These directions are in agreement with the direction of the active fault zones in the Aegean area, which are the result of the westward escape of the Anatolian Plate, as well as to the NNW–SSE extension in the broader Aegean area (e.g. McKenzie 1972).

As the depth increases, an increase in *S*-wave velocity is also observed. For the depth range from 16 to 20 km, a mean *S*-wave velocity around 3.5 km s^{-1} is found. Negative anomalies, that is, *S*-wave velocities lower than the mean value, are recognized in western Greece, whereas positive anomalies are depicted in northern and southern Aegean sea, suggesting that in these regions the lower crust has already been reached. The low-velocity zone in western Greece seems to follow the direction of the geological zones in this area, but the relatively poor path density in this area does not allow its accurate determination.

For the depths ranging from 20 to 26 km, the depicted *S*-wave velocities in the largest part of the Aegean sea, as well as for the eastern continental Greece, represent typical velocities of the lower crust (3.6–3.8 km s^{-1}). On the contrary, larger *S*-wave velocities (4.1–4.2 km s^{-1}) are observed in the SE Aegean sea, which are indicative of the uppermost mantle in this area. Similar *S*-wave velocities have been observed by Kalogeras (1993) along three paths that cross the south Aegean sea (Karpathos–Athens, Rhodes–Athens, and SW Turkey—Athens). In western Greece, the observed *S*-wave velocities probably depict the upper—lower crust boundary.

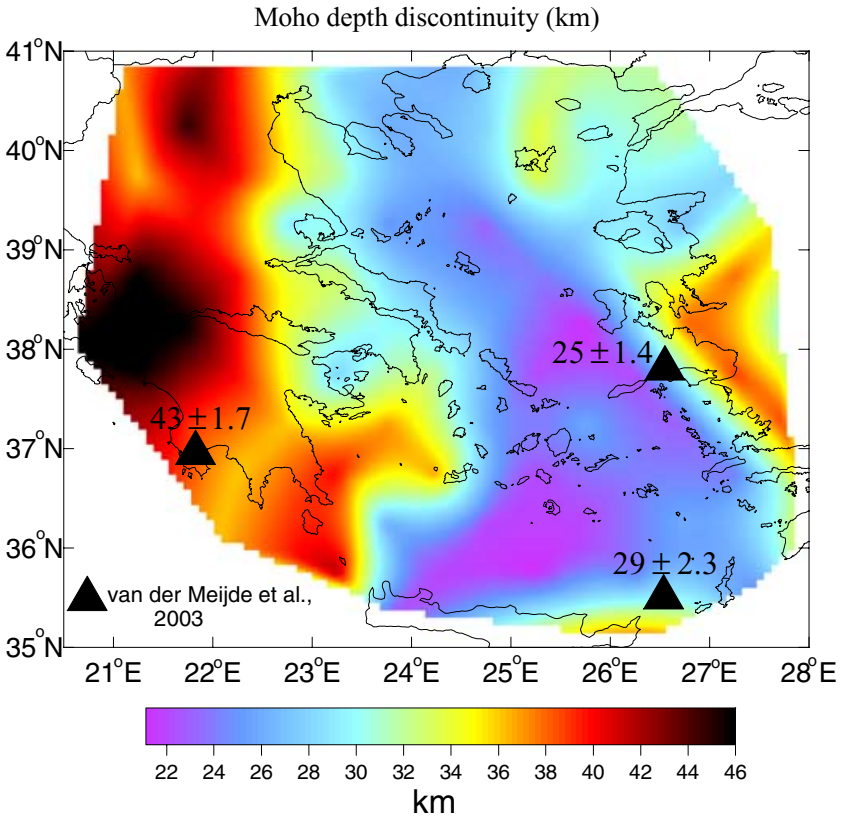

Figure 6. Crustal thickness (in km) for the broader Aegean area estimated in this work. The black triangles denote the locations that the Moho depth discontinuity has been calculated by the work of van der Meijde *et al.* (2003) and for each point this depth with its error is shown.

Up to the depth of approximately 30 km, *S*-wave upper-mantle velocities (4.0–4.3 km s^{-1}) dominate in the whole of the Aegean sea, whereas crustal *S*-wave velocities ($\sim$ 3.5 km s^{-1}) are observed in western Greece, indicating the presence of a thicker crust in this region, suggesting that a clear difference in crustal thickness between continental Greece and the Aegean sea is identified by our data.

For depths ranging from 30 to 40 km, very low *S*-wave velocities (3.6–3.8 km s^{-1}) extend over the southern and the central Aegean sea. These velocities, which are found just below the Moho discontinuity, can be correlated with the high heat flow in the mantle wedge above the subducted slab and the related active volcanism in the area, in agreement with body wave tomographic results (Spakman 1986; Spakman *et al.* 1993; Papazachos & Nolet 1997). The low *S*-wave velocity anomalies in the mantle wedge ($\sim$ 10 per cent, locally up to $\sim$ 14 per cent) obtained in the present study ($V_S \sim$ 3.7–3.8 km s^{-1}) in combination with the *P*-wave velocity anomalies from body wave tomography ($\sim$ 5–6 per cent, locally 7 per cent with V_P $\sim$ 7.3–7.4 km s^{-1}) correspond to an unusually high V_P/V_S ratio of 1.9–1.95, locally perhaps reaching 2.0. Such low velocities and high V_P/V_S values are usually attributed to the presence of partial melt in the mantle wedge and correspond to unusually high melt fractions of the order of 15–20 per cent for a typical mantle composition (e.g. Birch 1969). Surprisingly, petrogenetic results from volcanics of Santorini Island (Zelimer 1998) also suggest that a high degree of mantle melting of 15–20 per cent is present beneath the volcanic arc in the Aegean area. It is well known that the water flux as well as other volatiles that are released from the slab are very important to the amount of the partial melting. However, MELTS modelling (Zelimer 1998) indicates that too low H_20 is contained in basalts so the amount of water flux into the melting region beneath the Aegean arc is also too low to generate more than a few per cent of mantle melting (Davies & Bickle 1991). In consequence, only the hydrous fluxing of the mantle wedge cannot account for the relatively large degrees of mantle melting (15–20 per cent) as indicated by trace element constraints and the results of the present work. Hence, unless other volatiles such as CO_2 are released from the slab and increases melt production, melting beneath Santorini may at least in part be a result of the manifestation of the mantle diapers associated with the ascending flow of subduction-induced convection in the mantle wedge. It should be pointed out that the subducted sediments that also contain much of pore fluids contribute to the mantle melting only with a small amount of 0.2–0.4 per cent, while the slab fluids contribute 35–85 per cent of the fluid mobile element budget (Zelimer 1998).

A similar sequence of velocities, associated to a mantle wedge related to subduction, has been detected along the active (seismically and volcanically) side of the Tyrrhenian sea and bordering land (Panza *et al.* 2002; Pontevivo & Panza 2002). A low-velocity layer of *S* waves, at a depth of approximately 30 km, has also been detected by Kalogeras & Burton (1996) along three paths (Karpathos–Athens, Rhodes–Athens, and SW Turkey—Athens) that cross the southern Aegean sea. The *S*-wave velocities determined for this depth range suggest that in western Greece the lower crust has been reached, whereas mantle *S*-wave velocities (4.2–4.4 km s^{-1}) are detected in the south Peloponnesus.

For depths greater than 40 km a limited number of inversion results for the Aegean area are available, because our experimental data (group velocities) can not resolve the *S*-wave structure for depths greater than 50 km. However, they suggest that the *S*-wave

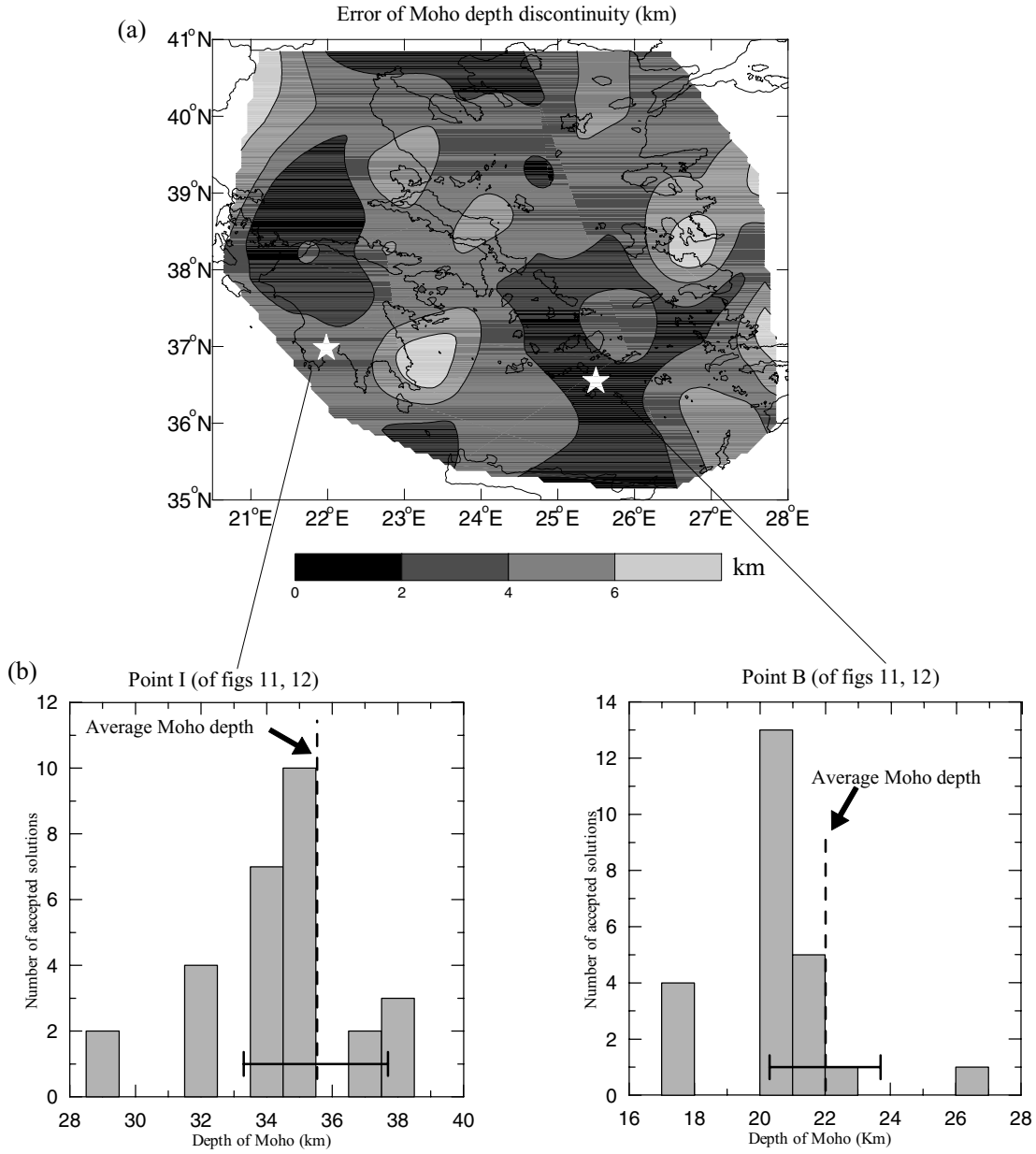

Figure 7. (a) Estimated error (in km) of the Moho discontinuity. (b) Histograms of the depths of Moho discontinuity for two typical gridpoints (I and B, Fig 12) in the Peloponnesus and the southern Aegean sea and the average value of Moho discontinuity with its error bar.

velocities determined in central and western Greece show typical uppermost mantle velocities.

In order to have a more detailed view of the velocity structure in the study area, the *S*-wave velocity contrast between the depths of 28 and 38 km is plotted in Fig. 9. In the central and southern Aegean sea, a well-defined upper-mantle low-velocity zone (mantle wedge low-velocity zone: MW LVZ) can be identified. This low-velocity zone near the active volcanism (black triangles) can be attributed to the rise of hot material from the asthenosphere in the Aegean area, as a result of the subduction of the African Plate under the Eurasian Plate. Our data are not adequate to accurately determine the bottom of this low-velocity zone, which is probably the high-velocity subducted slab (e.g. Spakman *et al.* 1988; Papazachos & Nolet 1997). Another low-velocity zone below the Chalkidiki peninsula can also be identified, in accordance with Christodoulou and Hatzfeld (1988) who detected a similar low-velocity zone in the *P*-wave structure at a depth of approximately 35–40 km, whereas later Papazachos & Scordilis (1998) confirmed the existence of this layer in *P*- as well as in *S*-wave structure.

Figs 10 and 11 depict several vertical cross-sections of the preferred 3-D shear wave velocity, where the estimated Moho discontinuity is shown as a black solid line and its uncertainty with the dashed lines. In Fig. 12, the results of the Hedgehog inversion, which has been performed at the examined gridpoints (A to M) along the two cross-sections of Fig. 11, are presented. For each gridpoint, using all the solutions (thin lines), we have estimated our preferred solution as the averaged solution (dotted line). In the same figure, the investigated parameters space (grey area) is shown. For the cross-section in Fig. 11(a), which has been obtained from the averaged solutions at points A to G, the inversion results (Fig. 12) show a clear mantle

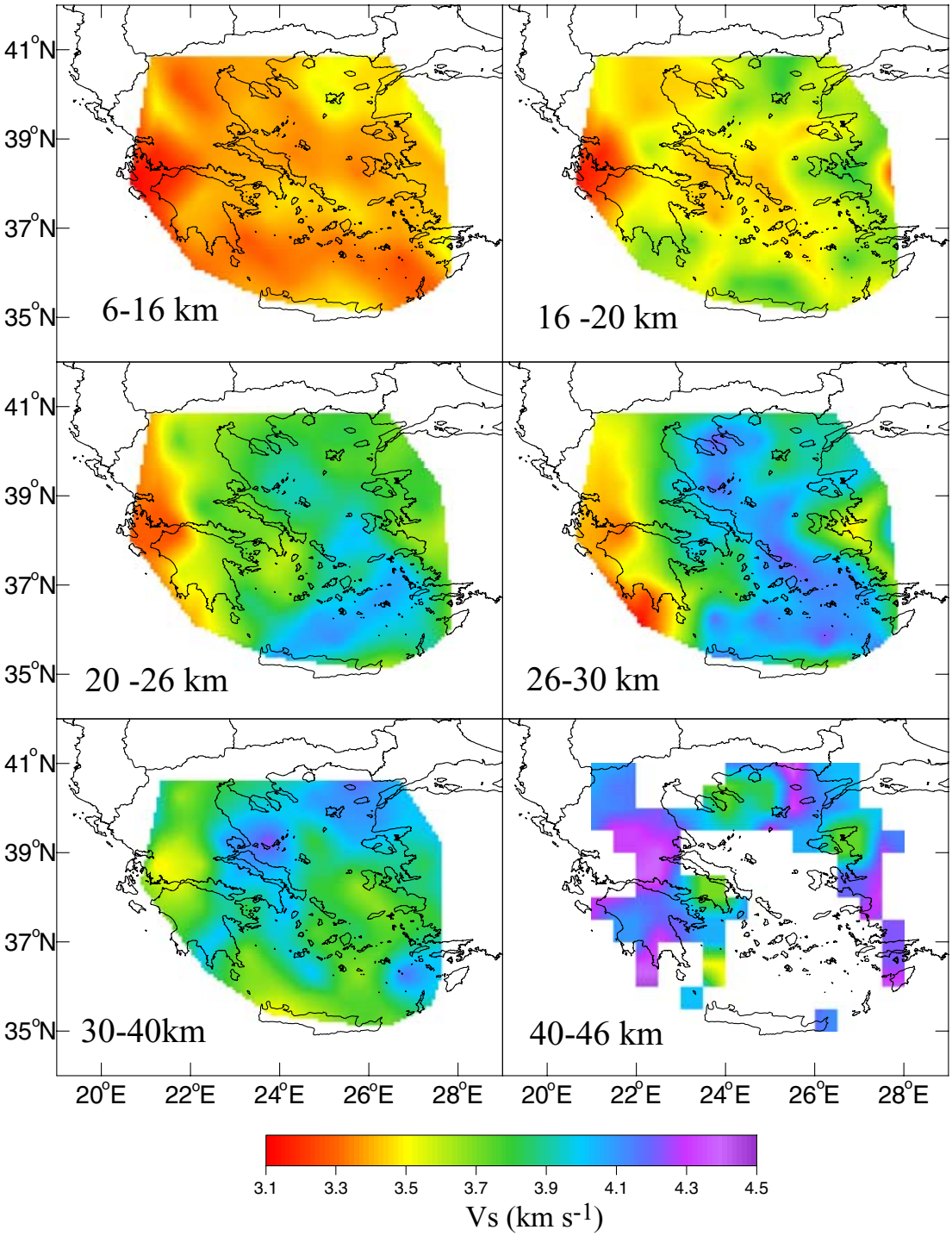

Figure 8. Horizontal cross-sections of the final shear wave velocity model for different depth ranges in the Aegean area.

low-velocity layer (MW LVZ) just north of Crete, which seems to continue in the southern Aegean sea and disappears to the north. A crustal low-velocity zone (C LVZ) appears locally in the depth range from 10 to 15 km at the second cross-section (Fig. 11b), which has been obtained from the averaged solutions (Fig. 12) at points H to M. The results presented in Fig. 12 show that for many gridpoints the low-velocity layers (e.g. in the upper crust for models A, H, I, or in the upper mantle for models B and D) are robust features and no solutions exist without their presence, though with different velocity contracts. However, in other cases (e.g. upper-mantle low-velocity layer for model C) some solutions without this MW LVZ are also found. On the other hand, even in these cases, the general trend of the majority of velocity models (e.g. see solutions for model C in Fig. 12 for depths larger than 30 km) strongly suggests a decrease of velocity with depth. Therefore, although the absence of MW LVZ can not be rigorously excluded as a possibility, it should be considered as very unlikely to occur.

The vertical cross-sections confirm that the approximate crustal thickness is 20–22 km in the southern and the central Aegean sea (Figs 10a , b and 11a), approximately 35 km south of Peloponnesus

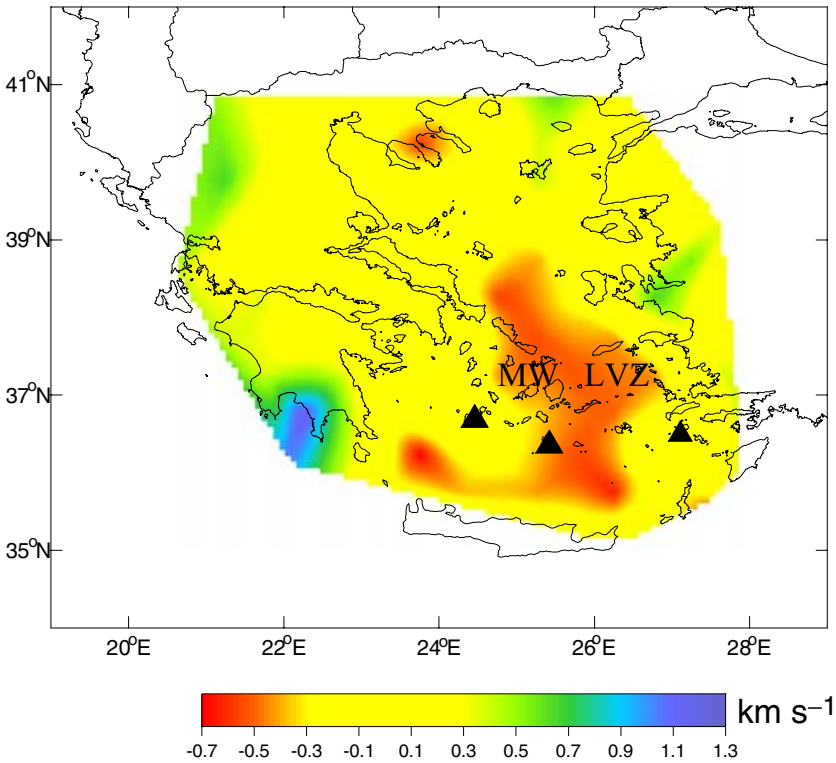

Figure 9. *S*-wave velocity contrast between 28 and 38 km for the final 3-D *S* velocity model. Negative values (<-0.2 km s^{-1}) define the low-velocity layer in the south Aegean sea and black triangles denote the most active volcanoes.

and near Rhodes island (Fig. 10a), 40–45 km in north Peloponnesus and in the western coast of Asia Minor (Fig. 10b), approximately 36 km in northwestern Greece and in central Greece (Figs 10c and 11b), around 25 km in the north Aegean sea near the Sporades islands (Fig. 10c) and 30–34 km in the north Aegean sea close to Lemnos island (Figs. 10c and 11a).

The mantle low-velocity zone (MW LVZ) that has been detected in the southern and central Aegaen sea for depths ranging from 30 to 40 km is visible in the vertical sections that cross the southern and the central Aegean sea (Figs 10a , b and 11a), whereas similarly low *S*-wave velocities do not appear in the north Aegean sea for the same depth range. At a depth of approximately 10–12 km a C LVZ is visible, mainly along the sedimentary Hellenic arc and Hellenides mountain range (Figs 10a , b, c and 11b) in western Greece, Peloponnesus and Dodekanese (Rhodes and Karpathos islands). The very low *S*-wave velocities that can be seen in the horizontal cross-sections in the northern Aegean sea, as well as in the Thermaikos gulf—Axios basin (Figs 11a and 10c) can be correlated to the significant thickness of sediments in the respective basins, approximately 6 km in the north Aegean sea (Kiriakidis 1988) and approximately 10 km in the centre of Axios basin (Sousounis 1993; Roussos 1994). These low *S*-wave velocities are in agreement with the work of Drakatos *et al.* (1989) who showed at the western borders of the Axios basin very low velocities in the shallow layers (∼15 km) and correlated them with the local geology of the area. (sedimentary basins and active tectonic–geothermal regions). The strong lateral variations of the crustal thickness and the shear velocities in the Aegean area are even more evident in the vertical sections of Fig. 11(a).

5 DISCUSSION AND CONCLUSIONS

The results of the surface wave tomography presented in this paper exhibit clear strong lateral variations in the Aegean area that can be correlated with known regional tectonic features. The most outstanding structural feature of the Aegean confirmed in this work is the crustal thickness difference between western Greece (along the Hellenides mountain range) and the Aegean sea (e.g. Fig. 11). In the southern Aegean sea, as well as in parts of the central Aegean sea, the crust has a thickness of approximately 20–22 km. This crustal thinning is associated with the extension tectonics of the Aegean backarc area and the rise of the mantle material, as a result of the convergence between the Eurasian and African plates. Generally, the inner Aegean sea shows a crustal thickness of less than 28–30 km, whereas in western Greece a significant crustal thickness of approximately 40–46 km is observed along the Hellenides mountain range. A normal crust of thickness of approximately 30–34 km is observed in eastern continental Greece. The results are in agreement with the Moho depth that has been derived by the work of van der Meijde *et al.* (2003) who showed a crustal thickness around 43 ± 1.7 km at one station located in west Peloponnesos, 25 ± 1.4 km for a station close to Samos Island and 29 ± 2.4 km at a station SW of Rhodes island. The results obtained in the present work show that the corresponding depths of Moho discontinuity are 39 ± 2.5, 24 ± 1.5 and 29 ± 2.2 km, respectively, in very good correlation with the aforementioned work of van der Meijde *et al.* (2003) as is shown in Figs 6 , 10 and 11.

Moreover, strong lateral variations of the shear wave velocity are exhibited in the constructed horizontal and vertical cross-sections

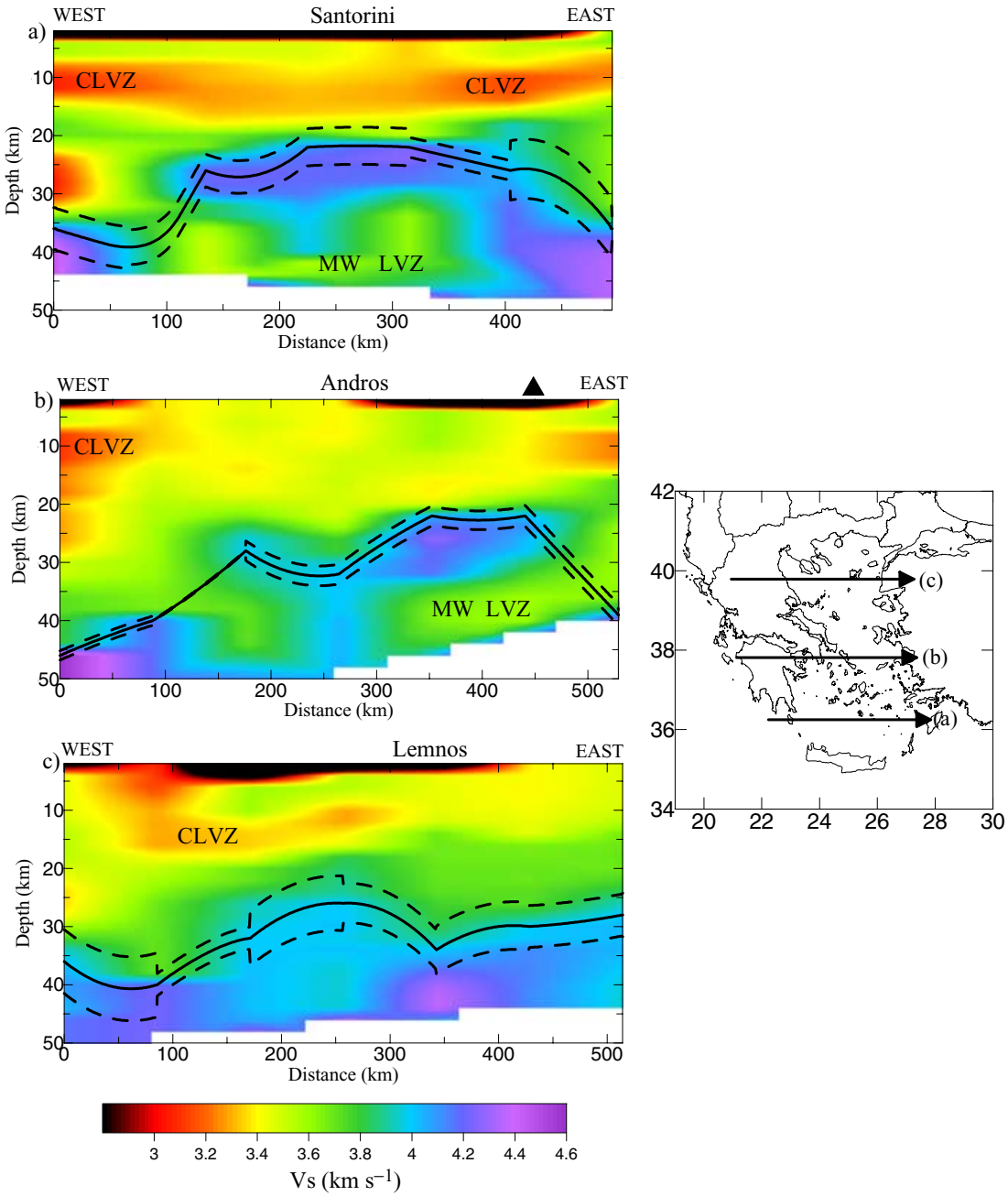

Figure 10. *S*-wave velocity distribution along three E–W trending cross-sections in the study area. The triangle shows the location that a Moho depth discontinuity has been calculated in the work of van der Meijde *et al.* (2003). The inset map on the right part of the figure indicates the location of the vertical sections.

passing through the Aegean area. In the depth range from 5 to 20 km, an *S*-wave low-velocity zone has been detected in western Greece, mainly under Peloponnesus and Rhodes. This low-velocity zone, which was first observed by Papazachos (1994) and Papazachos *et al.* (1995) and later confirmed by Papazachos & Nolet (1997), extends along the Hellenic arc and can be correlated to the Hellenides mountain range and the Alpine orogenesis, in accordance with the ideas of weakening mid-crustal intrusions and the associated LVZ (low-velocity zone) which was proposed by Mueller (1977). Previous studies detected this C LVZ only in the *P*-wave structure, as a result of the limited resolution of the *S*-wave traveltime data.

In the southern Aegean sea, as well as in a part of the central Aegean sea, the observed low *S*-wave velocities (3.6–3.8 km s^{-1}) at sub-Moho depths (30–40 km) indicate the presence of a low-velocity mantle wedge (MW LVZ) above the subducted slab. In the remaining part of the Aegean sea and in continental Greece the uppermost mantle is characterized by velocities around 4.3–4.4 km s^{-1}, slightly lower than previously published values based on body wave travel-time inversions (e.g. Papazachos & Nolet 1997).

The very low *S*-wave velocity anomaly that is shown in the mantle wedge (associated with the partial melting in the southern Aegean sea) has also been observed in similar geotectonic environments. Zhao *et al.* (1997) showed low P velocity anomalies (using body wave tomography) beneath the Tonga arc and the Lau backarc extending from the surface to approximately 100–140 km depth, where the primary magma genesis is expected to take place beneath an

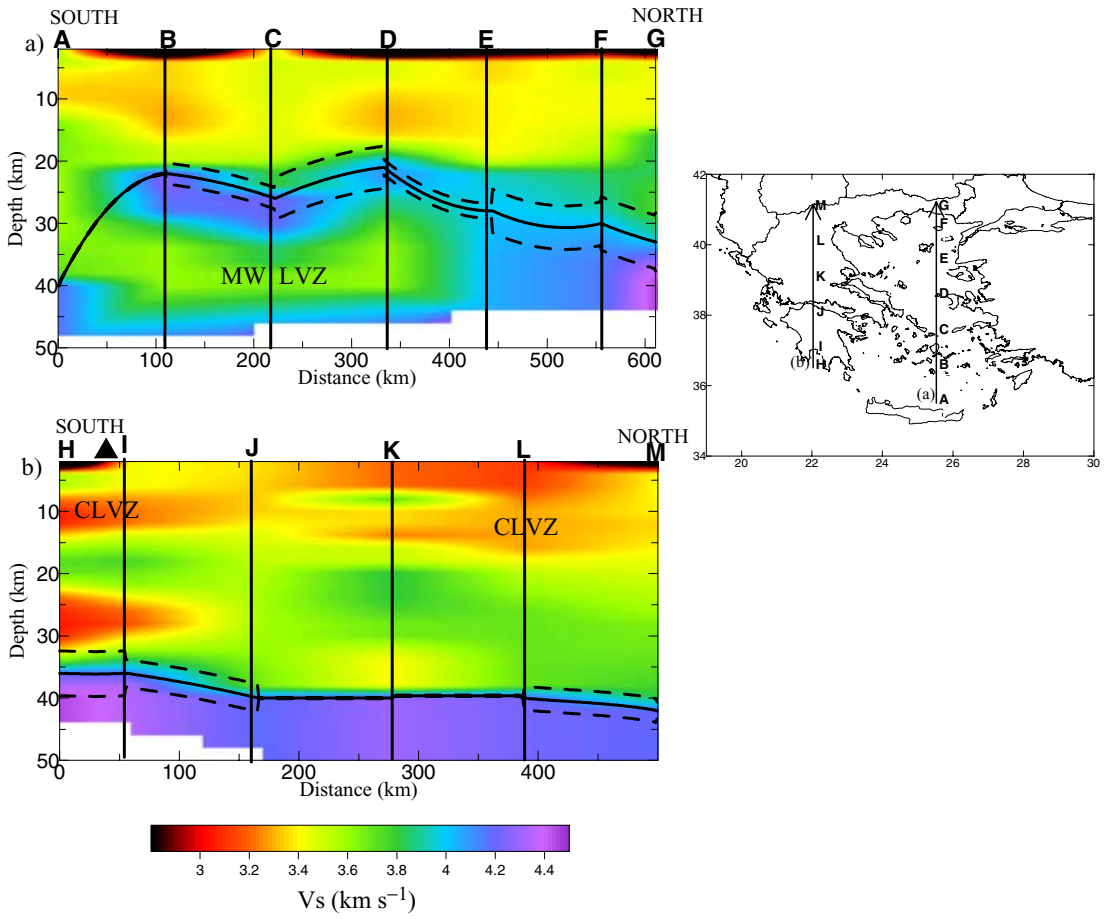

Figure 11. *S*-wave velocity distribution along two N–S trending cross-sections in the study area. The triangle shows the location that a Moho depth discontinuity has been calculated in the work of van der Meijde *et al.* (2003). The inset map on the right part of the figure indicates the location of the vertical sections. Points A to M are the centres of 0.5° × 0.5° cells where the Hedgehog inversion has been performed.

oceanic spreading centre. Moreover, they inverted 16 waveforms from 7 regional earthquakes recorded at the land stations to determine the 1-D *S*-wave velocity structure beneath the spreading centres. The inversion results showed a similar heterogeneity of *S* velocity (∼ 18 per cent, while the *P*-wave tomography showed 13 per cent) and a depth distribution of the backarc *S* velocities anomalies similar to that of the *P*-wave tomography. At the depth of approximately 40 km (up to 100–140 km), low *S*- wave velocities ∼ 3.8 km s^{-1} were found, similar to those found in our work for the mantle wedge. A similar low velocity anomaly has also been found beneath the Alaska and Japan volcanic arc (Zhao *et al.* 1995, 1997), probably representing the source zone for island arc magmas.

The results obtained in the present study, besides confirming previous results have two additional important geotectonic implications.

(i) Our results suggest the presence of a thin crust (of the order of 22–28 km) throughout the whole Aegean sea area and not locally in the southern Aegean sea between the volcanic arc and Crete, where previous work (e.g. Makris 1976) has shown the presence of a very thin crust using different methods (e.g. refraction data). We should point out that the lack of permanent recording stations in central and northern Aegean have prohibited in the past the identification of this crustal thinning by standard tomographic methods. Only gravity data (Papazachos 1994; Tsokas & Hansen 1997) have indicated the presence of a thin crust ranging from 25 to 30 km throughout the whole Aegean sea.

(ii) Upper-mantle velocities for *S* waves in the southern Aegean drop to very low velocities just below the Moho within the mantle wedge, reaching 3.7–3.8 km s^{-1} with local extremes at 3.6 km s^{-1}, corresponding to mantle velocity anomalies of 10 per cent and locally of 14 per cent. Such very low *S*-wave mantle-wedge velocities have not been computed before because no detailed regional surface wave tomographic results have been presented earlier, while very few results using *S*-wave traveltime tomography exist. Papazachos & Nolet (1997) showed low *S* velocities up to ∼ 4–5 per cent (locally ∼ 6 per cent), probably resulting from the *P*–*S* coupling imposed by the Poisson-ratio damping they used. These very low *S*-wave velocities, in combination with the well-known, from *P*-wave tomography (Spakman 1986; Spakman *et al.* 1988; Papazachos *et al.* 1995; Papazachos & Nolet 1997; Tiberi *et al.* 2000), *P*-velocity anomalies (upper-mantle velocity anomalies of the order or 6 per cent), have important implications on the geophysical conditions of the mantle wedge.

ACKNOWLEDGMENTS

The data collection for this work was partly supported by the E.C. projects ENV4-CT96-0277 and EVR1-CT-2001-40021 and by MIUR Cofinaziamento 2001 funds. Part of this work was done while EEK was an Erasmus-Socrates fellowship student at the

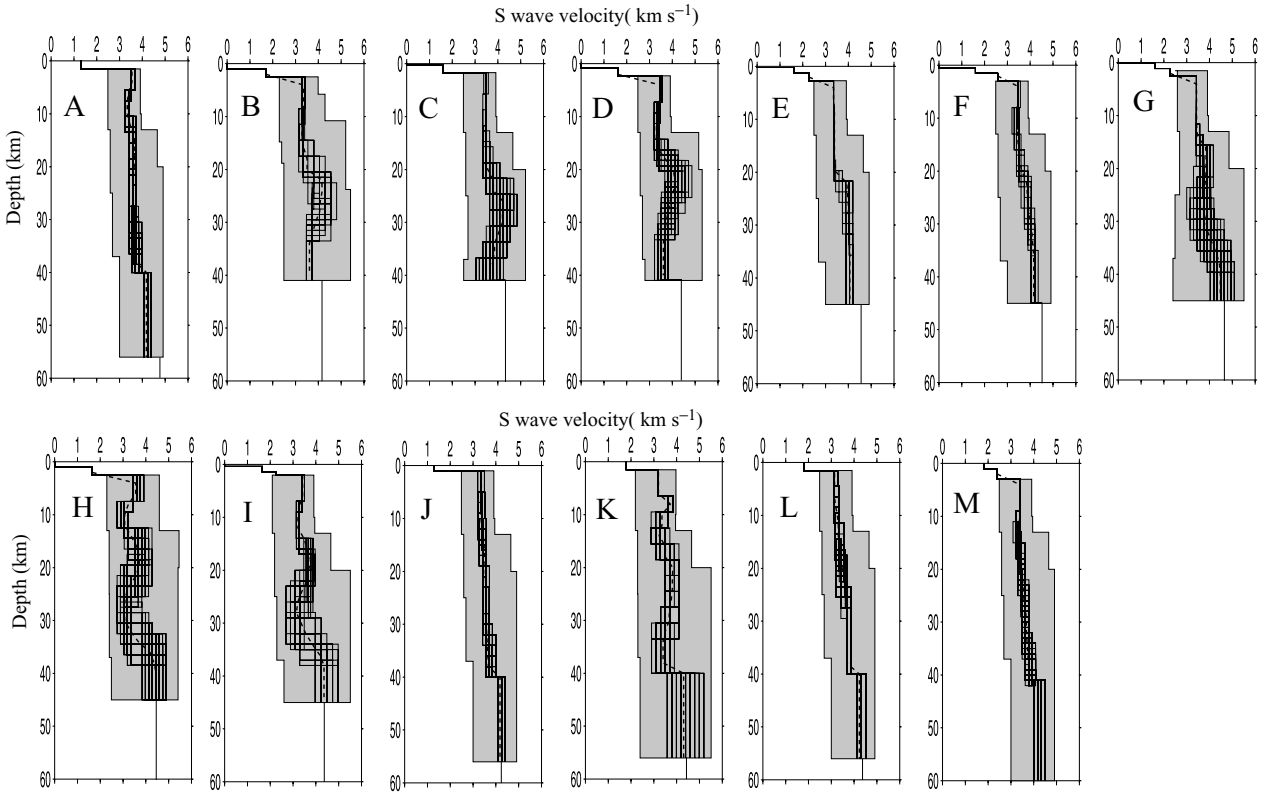

Figure 12. Set of solutions (*S*-wave velocity as a function of depth plotted as thin lines), as obtained from the Hedgehog inversion of the mean dispersion curves at the centre of each cell $0.5^\circ \times 0.5^\circ$, which are denoted with the letters A to M. For each cell the average solution (dotted line) as well as the investigated parameters space (grey area) are shown.

University of Trieste, Italy. We are grateful to Professor Anatoli Levshin for providing the FTAN code and Professor T. Yanovskaya and P. Ditmar from the University of St. Petersburg, Russia, for providing the tomographic inversion program. We would also like to thank the GeoForschungsZentrums, Potsdam Germany for providing the records from their network in the south Aegean sea. Finally, we are grateful to Thanasis Karamesinis, Afroditi Karnassopoulou, Ioannis Kassaras, Georgios Kaviris, Eleni Louvari, Kiriaki Paulou and Kiriakos Peftitselis for their help in the field work. EEK would also like to thank the Greek State Scholarship Foundation (GSSF) for its financial support through a 1996–1999 SSF scholarship.

REFERENCES

Anderson, H. & Jackson, J., 1987. Active tectonics of the Adriatic Region, *Geophys. J. R. astr. Soc.,* **91,** 937–983.

Backus, G. & Gilbert, F., 1968. The resolving power of gross Earth data, *Geophys. J. R. astr. Soc.,* **16,** 169–205.

Barton, P.J., 1986. The relationship between seismic velocity and density in the continental crust—a useful constraint?, *Geophys. J. R. astr. Soc.,* **87,** 195–208.

Birch, F., 1969. Density and Composition of the Upper Mantle: First Approximation as an Olivine Layer, in the Earth's Crust and Upper Mantle, pp. 18–36.

Biswas, N.N. & Knopoff, L., 1974. The structure of the upper mantle under the United States from the dispersion of Rayleigh waves, *Geophys. J. R. astr. Soc.,* **36,** 515–539.

Bohnhoff, M., Makris, J., Papanikolaou, P. & Stavrakakis, G., 2001. Crustal investigation of the Hellenic subduction zone using wide aperture seismic data, *Tectonophysics,* **343,** 239–262.

Brooks, M. & Kiriakidis, L., 1986. Subsidence of the North Aegean Trough: An alternative view, *J. geol. Soc. Lond.,* **143,** 23–27.

Calcagnile, G. & Panza, G.F., 1980. The main characteristics of the lithosphere–asthenosphere system in Italy and surrounding regions, *Pure appl. Geophys.,* **119,** 865–879.

Calcagnile, G., D'Ingeo, F., Farrugia, P. & Panza, G.F., 1982. The lithosphere in the central-eastern Mediterranean area, *Pure appl. Geophys.,* **120,** 389–406.

Caputo, M., Panza, G.F. & Postpischl, D., 1970. Deep structure of the Mediterranean basin, *J. geophys. Res.,* **75,** 4919–4923.

Chailas, S., Hipkin, R.G. & Lagios, E., 1993. Isostatic studies in the Hellenides. 2nd Congress of the Hellenic Geophysical Union, 5–7 May, Florina, Macedonia, Greece, pp. 492–504.

Christodoulou, A. & Hatzfeld, D., 1988. Three-dimensional crustal and upper mantle structure beneath Chalkidiki (northern Greece), *Earth planet. Sci. Lett.,* **88,** 153–168.

Davies, J.H. & Bickle, M.J., 1991. A physical model for the volume and composition of melt produced by hydrous fluxing above subduction zones, *Phil. Trans. R. Soc. Lond., A.,* **335,** 355–364.

Delibasis, N., Makris, J. & Drakopoulos, J., 1988. Seismic investigation of the crust and the upper mantle in western Greece, *Annal. Geol. Pays Hell.,* **33,** 69–83.

Ditmar, P.G. & Yanovskaya, T.B., 1987. A generalization of the Backus-Gilbert method for estimation of lateral variations of surface wave velocity, *Izvestia Acad. Sci. USSR,* **23**(6), 470–477.

Drakatos, G., 1989. Seismic tomography-Determination of high and low-velocity zones beneath Greece and surrounding regions, PhD thesis, p. 144, Univ. of Athens, Athens, Greece.

Drakatos, G. & Drakopoulos, J., 1991. 3-D velocity structure beneath the crust and upper mantle of the Aegean sea region, *Pure appl. Geophys.,* **135,** 401–420.

Drakatos, G., Latoussakis, J., Stavrakakis G., Papanastasiou, D. & Drakopoulos, J., 1989. 3-Dimensional velocity structure of the

north-central Greece from inversion of travel times. In: *3rd Congress of the Geological Society of Greece,* Geol. Soc. of Greece, Athens, **Vol. XXIII/3,** pp. 157–172.

Fleischer, U., 1964. Schwerestorungen im ostlichen Mittelmeer: nach Messungen mit einem Askania-Seegravimeter, *Deutschen Hydrogr. Zeitshr,* **7**(4), 153–164.

Fytikas, M., Innocentri, F., Manetti, P., Mazzuoli, R., Peccerillo, A. & Villari, L., 1985. Tertialy to Quaternary evolution of the volcanism in the Aegean region, in *The Geological Evolution of the Eastern Mediterranean,* Special Publication 17, eds Dixon, J.E. & Roberston, A.H., Geological Society, London, **Vol. 17,** pp. 687–699.

Gok, R., Turkelli, N., Sandvol, E., Seber, D. & Barazangi, M., 2000. Regional wave propagation in Turkey and surrounding regions, *Geophys. Res. Lett.,* **27,** 429–432.

Georgalas, G., 1962. *Catalogue of the Active Volcanoes and Solfatara Fields in Greece,* Part 12, International Association of Volcanology, Rome.

Hashida, T., Stavrakakis, G. & Shimazaki, K., 1988. Three-dimensional seismic attenuation beneath the Aegean region and its tectonic implication, *Tectonophysics,* **145,** 43–54.

Hatzfeld, D. *et al.*, 2001. Shear wave Anisotropy in the upper mantle beneath the Aegean related to internal deformation, *J. geophys. Res.,* **106**(B12), 30 737–30 753.

Jackson, J., 1994. Active tectonics of the Aegean region, *Annu. Rev. Earth planet. Sci.,* **22,** 239–271.

Kalogeras, J.S., 1993. A contribution of surface seismic waves in the study of the crust and upper mantle in the area of Greece, *PhD thesis*, Univ. of Athens, Athens, Greece, pp. 1–186.

Kalogeras, J.S. & Burton, P.W., 1996. Shear-wave velocity models from Rayleigh-wave dispersion in the broader Aegean area, *Geophys. J. Int.,* **125,** 679–695.

Karagianni, E.E. *et al.*, 2002. Rayleigh wave group velocity tomography in the Aegean area, *Tectonophysics,* **358,** 187–209.

Keilis-Borok, V.I. & Yanovskaya, T.B., 1967. Inverse problems of seismology, *Geophys. J. R. astr. Soc.,* **13,** 223–234.

Kiratzi, A.A., Papadimitriou, E.E. & Papazachos, B.C., 1987. survey in the Steno dam site in northwestern Greece, *Ann. Geophys.,* **5,** 161–166.

Kiriakidis, L.G., 1988. The Vardar ophiolite: a continous belt under the Axios basin sediments, *Geophys. J. Int.,* **98,** 203–212.

Knopoff, L., 1964. A matrix method for elastic wave problems, *Bull. seism. Soc. Am.,* **54,** 431–438.

Knopoff, L., 1972. Observation and inversion of surface wave dispersion, *Tectonophysics,* **13,** 497–519.

Le Pichon, X. & Angelier, J., 1979. The Hellenic arc and trench system: A key to the neotectonic evolution of the eastern Mediterranean area, *Tectonophysics,* **60,** 1–42.

Levshin, A.L., Ratnikova, L.I. & Berteussen, K.A., 1972. On a frequency-time analysis of oscillations, *Ann. Geophys.,* **28,** 211–218.

Levshin, A.L., Yanovskaya, T.B., Lander, A.V., Bukchin, B.G., Barmin, M.P., Ratnikova, L.I. & Its, E.N., 1989. Recording, identification and measurement of surface wave parameters, in *Seismic surface waves in a laterally inhomogeneous Earth,* pp. 131–182, ed. Keilis-Borok, V.I., Kluwer Academic Publisher, Dordrecht.

Levshin, A.L., Ratnikova, L.I. & Berger, J., 1992. Peculiarities of surface-wave propagation across central Eurasia, *Bull. seism. Soc. Am.,* **82,** 2464–2493.

Ligdas, C.N. & Lees, J.M., 1993. Seismic velocity constrains in the Thessaloniki and Chalkidiki areas (northern Greece) from a 3-D tomographic study, *Tectonophysics,* **228,** 97–121.

Ligdas, C.N. & Main, I.G., 1991. On the resolving power of tomographic images in the Aegean area, *Geophys. J. Int.,* **107,** 197–203.

Ligdas, C.N., Main, I.G. & Adams, R.D., 1990. 3-D structure of the lithosphere in the Aegean sea region, *Geophys. J. Int.,* **102,** 219–229.

McClusky, S. *et al.*, 2000. Global Positioning System constraints on plate kinematics and dynamics in the eastern Mediterranean and Caucasus, *J. geophys. Res.,* **105,** 5695–5719.

McKenzie, D.P., 1970. The plate tectonics of the Mediterranean region, *Nature,* **226,** 239–243.

McKenzie, D.P., 1972. Active tectonics of the Mediterranean region, *Geophys. J. R. astr. Soc.,* **30,** 109–185.

McKenzie, D.P., 1978. Active tectonics of the Alpine-Himalayan belt: The Aegean sea and surrounding regions, *Geophys. J. R. astr. Soc.,* **55,** 217–254.

Makris, J., 1973. Some geophysical aspects of the evolution of the Hellenides, *Bull. geol. Soc. Greece,* **10,** 206–213.

Makris, J.A., 1976. A dynamic model of the Hellenic arc deduced from geophysical data, *Tectonophysics,* **36,** 339–346.

Makris, J.A., 1977. Geophysical investigation of the Hellenides, *Geophys. Einzelschr. Hamburger,* Heft 27: 1–98.

Makris, J.A., 1978. The crust and upper mantle of the Aegean region from deep seismic soundings, *Tectonophysics,* **46,** 269–284.

Marquering, H. & Snieder, R., 1996. Shear-wave velocity structure beneath Europe, the northeastern Atladic and western Asia from waveform inversions including surface-wave mode coupling, *Geophys. J. Int.,* **127,** 283–304.

Martin, L., 1987. Structure et evolution recente de la Mer Egee, *PhD Thesis*, Univ. Paris-Sud, p. 305.

Martinez, M.D., Lana, X., Canas, J.A., Badal, J. & Pujades, L., 2000. Shear-wave velocity tomography of the lithosphere–asthenosphere system beneath the Mediterranean area, *Phys. Earth planet. Int.,* **122,** 33–54.

van der Meijde, M., van der Lee, S. & Giardini, D., 2003. Crustal structure beneath broad-band seismic stations in the Mediterranean region, *Geophys. J. Int.,* **152,** 729–739.

Mueller, St., 1977. A new model of the continental crust, in *The Earth's Crust: its Nature and Physical Properties,* Vol. 20, pp. 289–317, ed. Heacock, J.G., AGU, Washington, DC.

Panagiotopoulos, D.G., 1984. Travel time curves and crustal structure in the southern Balkan region, PhD thesis, Univ. of Thessaloniki, Thessaloniki, p. 159 (in Greek).

Panagiotopulos, D.G. & Papazachos, B.C., 1985. Travel times of Pn waves in the Aegean and surrounding area, *Geophys. J. R. astr. Soc.,* **80,** 165–176.

Panza, G.F., 1981. The resolving power of seismic surface waves with respect to crust and upper mantle structural models, in *The solution of the Inverse Problem in Geophysical Interpretation,* pp. 39–77, ed. Cassinis, R., Plenum Press, New York.

Panza, G.F., Pontevivo, A., Sarao', A., Aoudia, A. & Peccerillo, A., 2002. Structure of the lithosphere–asthenosphere and Volcanism in the Tyrrhenian Sea and surroundings, Mem. Desc. Carta. Geol. d'It., XLIV, 29–56.

Papazachos, B.C., 1969. Phase velocities of Rayleigh waves in southeastern Europe and eastern Mediterranean sea, *Pure appl. Geophys.,* **75,** 47–55.

Papazachos, B.C. & Comninakis, P.E., 1969. Geophysical features of the Greek islands Arc and Eastern Mediterranean Ridge, *Com. Ren. Seances Conf. Reunie Madrid,* **16,** 74–75.

Papazachos, B.C. & Comninakis, P.E., 1971. Geophysical and tectonic features of the Aegean arc, *J. geophys. Res.,* **76,** 8517–8533.

Papazachos, B.C. & Papazachou, C.B., 1997. *The Earthquakes of Greece,* Ziti Publ., Thessaloniki, Greece, p. 304.

Papazachos, B.C., Polatou, M. & Mandalos, N., 1967. Dispersion of surface waves recorded in Athens, *Pure appl. Geophys.,* **67,** 95–106.

Papazachos, B.C., Kiratzi, A., Hatzidimitriou, P. & Rocca, A., 1984. Seismic faults in the Aegean area, *Tectonophysics,* **106,** 71–85.

Papazachos, B.C., Papadimitriou, E.E., Kiratzi, A.A., Papazachos, C.B. & Louvari, E.K., 1998. Fault plane solutions in the Aegean sea and the surrounding area and their tectonic implications, *Bolletino di Geofisica Teorica ed Applicata,* **39,** 199–218.

Papazachos, B.C., Dimitriadis, S.T., Panagiotopoulos, D.G., Papazachos, C.B. & Papadimitriou, E.E., 2004. Deep structure and active tectonics of the Southern Aegean Volcanic arc. In:, *The International, Conference: The South Aegean Active Volcanic Arc: Present Knowledge and Feature Perspectives (SAAVA 2003)*, Milos Conference Center, Milos Island, Greece, 17–20 September 2003, in Elsevier's Book Series: Developments in Volcanology 'The South Aegean Active Volcanic Arc: Present Knowledge and Future Perspectives', in press.

Papazachos, C.B., 1994. Structure of the crust and upper mantle in SE Europe by inversion of seismic and gravimetric data, PhD thesis, Univ. of Thessaloniki, Greece (in Greek).

Papazachos, C.B., 1998. Crustal and upper mantle P and S velocity structure of the Serbomacedonian massif (Northern Greece), *Geophys. J. Lett.,* **134,** 25–39.

Papazachos, C.B., 1999. Seismological and GPS evidence for the Aegean-Anatolia interaction, *Geophys. Res. Lett.,* **17,** 2653–2656.

Papazachos, C.B. & Nolet, G., 1997. P and S deep structure of the Hellenic area obtained by robust nonlirear inversion of travel times, *J. geophys. Res.,* **102,** 8349–8367.

Papazachos, C.B. & Scordilis, E.M., 1998. Crustal structure of the Rhodope and surrounding area obtained by non-linear inversion of P and S travel times and its tectonic implications, *Acta Vulcanologica,* **10**(2), 339–345.

Papazachos, C.B., Hatzidimitriou, P.M., Panagiotopoulos, D.G. & Tsokas, G.N., 1995. Tomography of the crust and upper mantle in southeast Europe, *J. geophys. Res.,* **100,** 405–422.

Pasyanos, M.E., Walter, W.R. & Hazlert, S.E., 2001. A surface wave dispersion study of the Middle East and North Africa for Monitoring the Comprehensive Nuclear-Test-Ban treaty, *Pure appl. Geophys.,* **158,** 1445–1474.

Payo, G., 1967. Crustal structure of the Meditterranean sea by surface waves. Part I, Group velocity, *Bull. seism. Soc. Am.,* **57,** 151–172.

Payo, G., 1969. Crustal structure of the Meditterranean sea by surface waves. Part II, Phase velocity and travel times, *Bull. seism. Soc. Am.,* **59,** 23–42.

Plomerova, J., Babuska, V., Pujdusak, P., Hatzidimitriou, P., Panagiotopoulos, D., Kalogeras, J. & Tassos, S., 1989. Seismicity of the Aegean and surrounding areas in relation to topography of the lithospere-asthenosphere transition. In: *Proc. 4th Inter. Sym. Analysis Seismicity and Seismic Risk, Bechyne Chechoslavakia, Sep. 4–9*, pp. 209–215.

Pontevivo, A. & Panza, G.F., 2002. Group velocity tomography and regionalization in Italy and bordering areas, *Phys. Earth planet. Int.,* **4133,** 1–15.

Roussos, N., 1994. Stratigraphy and paleogeographic evolution of the Paleogene Molassic basins of the North Aegean area. In: *Proceedings of the 7th Congress of the Geological Society of Greece, Thessaloniki 25–27 May,* Vol. XXX/2, pp. 275–294, Geological Society of Greece, Thessaloniki.

Schwab, F.A. & Knopoff, L., 1972. Fast surface wave and free mode computations, in, *Methods in computational Physics,* pp. 86–180, ed. Bolt, B.A., Academic Press, New York.

Schwab, F.A., Nakanishi K., Cuscito M., Panza G.F. & Liang, G., 1984. Surface-wave computations and the synthesis of theoretical seismograms at high frequencies, *Bull. seism. Soc. Am.,* **74,** 1555–1578.

Scordilis, E.M., Karakaisis, G.F., Karacostas, B.G., Panagiotopoulos, D.G., Comninakis, P.E. & Papazachos, B.C., 1985. Evidence for transforming faulting in the Ionian Sea: the Cefalonia island earthquake sequence of 1983, *Pure appl. Geophys.,* **123,** 388–397.

Sousounis, G., 1993. Estimation of the hot dry rocks (HDR) with data from boreholes and seismic data. In: *2nd Congress of the Hellenic Geophysical Union, Florina, 5–7 May*, Florina, Greece, pp. 276–287.

Spakman, W., 1986. Subduction beneath Eurasia in connection with the Mesozoic Tethys, *Geol. Mijnbouw.,* **65,** 145–153.

Spakman, W., Wortel, M.J.R. & Vlaar, N.J., 1988. The Hellenic subduction zone: Atomographic image and its dynamic implications, *Geophys. Res. Lett.,* **15,** 60–63.

Spakman, W., Van der Lee, S. & Van der Hilst, R.D., 1993. Travel-time tomography of the European-Mediterranean mantle down to 1400 km, *Phys. Earth planet. Int.,* **79,** 3–74.

Taymaz, T., Jackson, J. & McKenzie, D., 1991. Active tectonics of the north central Aegean Sea, *Geophys. J. Int.,* **106,** 433–490.

Tiberi, C. *et al.*, 2000. Crustal and upper mantle structure beneath the Corinth rift (Greece) from a teleseismic tomography study, *J. geophys. Res.,* **105,** 28 159–28 171.

Tsokas, G.N. & Hansen, R.O., 1997. Study of the crustal thickness and the subducting lithosphere in Greece from gravity data, *J. geophys. Res.,* **102,** 20 585–20 597.

Urban, L., Cichowicz, A. & Vaccari, F., 1993. Computation of analytical partial derivatives of phase and group velocities for Rayleigh waves with respect to structural parameters, *Studia geoph. et geod.,* **37,** 14–36.

Valyus, V.P., 1968. Determining seismic profiles from a set of observations (in Russian), *Vychislitelnaya Seismologiya,* **4,** 3–14. English translation in Valyus, V.P., 1972. *Computational Seismology,* ed. Keilis-Borok, V.I., Consultants Bureau, New York, pp. 114–118.

Vogt, P. & Higgs, P., 1969. An aeromagnetic survey of the eastern Mediterranean sea and its interpretation, *Earth. planet. Sci. Lett.,* **5,** 439–448.

Voulgaris, N., 1991. Investigation of the crustal structure in western Greece (Zakinthos-NW Peloponessus area), PhD thesis, Univ. of Athens, Athens, Greece (in Greek).

Yanovskaya, T.B., 1997. Resolution estimation in the problems of seismic ray tomography, *Izvestia, Physics of the solid Earth,* **33**(9), 762–765.

Yanovskaya, T.B. & Ditmar, P.G., 1990. Smoothness criteria in surface wave tomography, *Geophys. J. Int.,* **102,** 63–72.

Yanovskaya, T.B., Kizima, E.S. & Antomova, L.M., 1998. Structure of the crust in the Black Sea and adjoining regions from surface wave data, *J. Seismology,* **2,** 303–316.

Zelimer, G.F., 1998. Petrogenetic processes and their timescales beneath Santorini, Aegean Volcanic Arc, Greece, PhD thesis, The Open University, Milton Keynes, UK.

Zhao, D., Christensen, D. & Pulpan, H., 1995. Tomographic imaging of the Alaska subduction zone, *J. geophys. Res.,* **100,** 6487–6504.

Zhao, D., Xu, Y., Wiens, D.A., Dorman, L., Hildebrand, J. & Webb, S., 1997. Depth Etent of the Lau Back-Arc Spreading Center and Its Relation to Subduction Processes, *Science,* **278,** 254–257.